Patient-Specific Left Ventricular Flow Simulations From Transthoracic Echocardiography: Robustness Evaluation and Validation Against Ultrasound Doppler and Magnetic Resonance Imaging

David Larsson, Jeannette H. Spühler, Sven Petersson, Tim Nordenfur, Massimiliano Colarieti-Tosti, Johan Hoffman, Reidar Winter, and Matilda Larsson

***Abstract*— The combination of medical imaging with computational fluid dynamics (CFD) has enabled the study of 3-D blood flow on a patient-specific level. However, with models based on gated high-resolution data, the study of transient flows, and any model implementation into routine cardiac care, is challenging. This paper presents a novel pathway for patient-specific CFD modelling of the left ventricle (LV), using 4-D transthoracic echocardiography (TTE) as input modality. To evaluate the clinical usability, two sub-studies were performed. First, a robustness evaluation was performed, where repeated models with alternating input variables were generated for six subjects and changes in simulated output quantified. Second, a validation study was carried out, where the pathway accuracy was evaluated against pulsed-wave Doppler (100 subjects), and 2-D through-plane phase-contrast magnetic resonance imaging measurements over seven intraventricular planes (6 subjects). The robustness evaluation indicated a model deviation of <12%, with highest regional and temporal deviations at apical segments and at peak systole, respectively. The validation study showed an error of <11% (velocities <10 cm/s) for all subjects, with no significant regional or temporal differences observed. With the patient-specific pathway shown to provide robust output with high accuracy, and with the pathway dependent only on 4-D TTE, the method has a high potential to be used within future clinical studies on 3-D intraventricular flow patterns. To this, future model developments in the form of e.g., anatomically accurate LV valves may further enhance the clinical value of the simulations.**

***Index Terms*— Transthoracic echocardiography, TTE, computational fluid dynamics, CFD, patient-specific, modelling, validation, robustness evaluation.**

Manuscript received May 5, 2017; revised June 13, 2017; accepted June 17, 2017. Date of publication July 21, 2017; date of current version October 25, 2017. This work was supported in part by the Swedish Research Council under Grant VR, 2015-04237 and in part by the Swedish Foundation for Strategic Research under Grant SSF, AM13-0049. *(Corresponding author: David Larsson.)*

D. Larsson and T. Nordenfur are with the Department of Medical Engineering, KTH Royal Institute of Technology, SE-10044 Stockholm, Sweden, and also with the Department of Clinical Sciences, Karolinska Institutet, SE-17177 Stockholm, Sweden (e-mail: david.larsson@sth.kth.se).

J. H. Spühler and J. Hoffman are with the Department of Computational Science and Technology, KTH Royal Institute of Technology, SE-10044 Stockholm, Sweden.

S. Petersson is with the Department of Diagnostic Medical Physics, Karolinska University Hospital, SE-17177 Stockholm, Sweden.

M. Colarieti-Tosti is with the Department of Medical Engineering, KTH Royal Institute of Technology, SE-10044 Stockholm, Sweden, and also with the Department of Clinical Science, Intervention and Technology, Karolinska Institutet, SE-17177 Stockholm, Sweden.

R. Winter is with the Department of Clinical Sciences, Karolinska Institutet, SE-17177 Stockholm, Sweden.

M. Larsson is with the Department of Medical Engineering, KTH Royal Institute of Technology, SE-10044 Stockholm, Sweden, and also with the Department of Molecular Medicine and Surgery, Karolinska Institutet, SE-17177 Stockholm, Sweden.

Color versions of one or more of the figures in this paper are available online at http://ieeexplore.ieee.org.

Digital Object Identifier 10.1109/TMI.2017.2718218

I. Introduction

IN THE ventricles of the healthy heart, the formation of vortices and vortex-like structures is a distinct flow feature [1], enabling for the continuous redirection of blood from filling to ejection. Consequently, 3D blood flow motion has been proposed as an important biomarker for predicting cardiovascular pathologies through observation of abnormal flow patterns [2], [3]. Importantly, such flow changes have even been suggested to occur before any significant and detectable morphological changes can be detected [4].

Several techniques have been developed to assess blood flow motion for diagnostic purposes. Ultrasound Doppler imaging is routinely used to evaluate e.g. the degree of valvular regurgitation [5] or stenosis [6]. However, in Doppler imaging only the flow component in the direction of the ultrasound beam is assessed, and in the presence of vortices the signal deteriorates. Promising developments have been made in the field of ultrasound flow imaging, where ultrafast compound Doppler imaging [7], synthetic aperture [8], or echocardiographic particle image velocimetry [9] have enabled measurement of the lateral flow component. However, any clinical implementation of these techniques remains to be performed, awaiting primarily large-scale validation.

In addition to ultrasound-based techniques, magnetic resonance imaging (MRI) can be used to quantify blood flow. Using 2D time-resolved (CINE) phase-contrast (PC) MRI the out-of-plane velocity component from a defined anatomical plane can be assessed [10]. The development of 4D flow cardiovascular MRI has further enabled the assessment of multidirectional blood flow motion [11]. However, an inherent issue with MRI-based flow measurements is the need for temporal gating, resulting in data averaged over a number of cardiac cycles (with scan times ranging from 5 to 25 minutes), limiting the ability to capture temporally fluctuating flows.

As an alternative, the use of computational fluid dynamics (CFD) in combination with medical imaging has emerged as a promising area for studying detailed flow phenomena. Using CFD simulations, highly resolved flow fields can be obtained at a level currently not achievable by imaging, and by including imaged-based anatomical boundary conditions, patient-specific CFD models can be created [12]–[14]. For patient-specific cardiac CFD, several groups have presented MRI-based models of the left ventricle (LV) [12], [13], as well as for the left atrium and ventricle [14]. Similarly, CT-based models have been created at a highly detailed level [15], [16]. However, both modalities come with certain limitations: MRI models require temporal gating and the ability to study non-periodic pathologies or transient cardiac events is limited. For CT models, the patient is exposed to a certain level of ionizing radiation, and the ability to derive a priori flow information at model boundaries is so far limited.

Instead, the use of ultrasound for patient-specific CFD modelling has been proposed as an alternative to overcome the aforementioned issues [17]. Firstly, echocardiography has high temporal resolution, with ultrafast acquisition schemes [18] promising even higher acquisition frequencies in the future. Secondly, echocardiography is widely available and is routinely used as the first point-of-care for patients suffering from cardiovascular disease. A patient-specific CFD pathway based on ultrasound imaging would thus have the potential to be directly connected to clinical practice [19].

Currently, only a few echocardiography-based CFD model frameworks have been published. Voigt *et al.* [20] presented one of the first, with input data acquired from transesophageal echocardiography (TEE). Similarly, Bavo *et al.* [21] recently presented a related approach, with the wall and mitral valve motion captured from TEE. However, TEE requires the insertion of a probe into the esophageal cavity, wherefore the use of such models in routine practice may be limited. Some work do exist using transthoracic echocardiography (TTE) to simulate the flow field of the LV [22], however in this case the patient-specific method was only applied in one patient case, and model validation was only performed in a simplified 2D case. In general, model validation is a pressing issue for all presented patient-specific CFD models of the LV. If any validation is attempted, most commonly only a qualitative one is performed [12], [13]. In the case of any quantification, such has either been performed in controlled *in-vitro* setups [23], [24] or against *in-vivo* measurements where only a sub-region of the LV was covered [20]. Thus, there is indeed a need for a thoroughly validated patient-specific cardiac CFD model, in particular one being based on echocardiography.

The aim of the following study can therefore be divided into three major parts. First, the aim is to develop a novel TTE-based patient-specific pathway for CFD simulations of the LV. Second, the study aims at quantifying the robustness of the simulations against variations in input variables. Third, a thorough validation of the simulated flow fields against patient-specific *in-vivo* flow measurements from both Doppler ultrasound and PC-MRI is performed in order to quantify the accuracy of the pathway. To our knowledge the work represents one of the first patient-specific CFD models of the LV with an extensive validation against multimodal *in-vivo* flow measurements. In combination with the pathway being based on TTE, the following work represents a novel and potentially important contribution to the field. Please note that the following paper represents a significant extension of previous published work by the same group, where preliminary studies of model robustness [25] and initial correspondence to *in-vivo* measurements [26] were performed.

II. Methodology

The following section is divided into three parts: *A*) *Patient-specific CFD simulations of the LV*, describing the methodological and technical details of the pathway, *B*) *Robustness evaluation*, quantifying the effect of alternating input parameters on the simulated LV flow, and *C*) *Validation against in-vivo flow measurements*, comparing simulated flows to Doppler and MRI-based *in-vivo* flow measurements.

For all outlined clinical measurements, all subjects participated under informed consent, with ethical approval granted by the Swedish Ethical Review Board (EPN, Dnr: 2015/1345-31/1) prior to the study initiation. The approval included acquisition and data handling of 4D echocardiography and PW Doppler at the LV valves during clinically induced echocardiography, as well as subsequent 2D through-plane PC-MRI measurements on a subset of consenting subjects. For specific measurement details, please see corresponding sections below.

A. Patient-Specific CFD Simulations of the LV

The following part outlines the major steps representing the proposed patient-specific model pathway. An overview of these is given in Figure 1.

1) Clinical Image Acquisition: 4D (sometimes denoted 3D+time) TTE images of the LV were acquired from a routine apical TTE view. The field of view was chosen to capture the movement of the LV endocardium throughout the entire cardiac cycle. Images were acquired using a GE Healthcare Vivid E9 (4VD, 1.7MHz/3.3MHz, 26-62 fps, equalling an axial resolution = 0.7 mm and a temporal resolution = 38-16 ms), with a field-of-view covering the entire LV throughout the cardiac cycle with maximum scan depth = 25 cm, and maximum opening angle = 80°.

2) Endocardial Segmentation: From the acquired 4DTTE images, the endocardial border of the LV was segmented in all time frames. This was achieved by delineating the endocardial border using the GE Healthcare 4D AutoLVQ

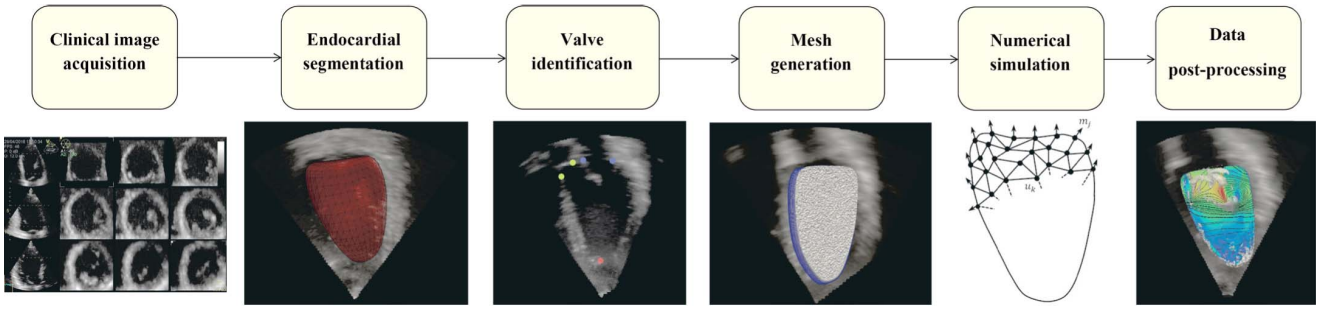

Fig. 1. Overview of pathway for patient-specific CFD simulations of the LV, illustrating all outlined steps from clinical image acquisition to data post-processing. As an example, the post-processing image is given for a subject with normal LV function with overlaid iso-streamlines and λ_2 iso-surfaces.

algorithm [27]. The algorithm works in a semi-automated fashion, where segmentation is computed from identified apical and central base position at end systole (ES) and end diastole (ED), respectively. A final segmented, triangulated surface mesh (approximately 642 nodes) is generated, capturing the time-dependent movement of the identified LV endocardial wall.

3) Valve Identification: The aortic and mitral valves, representing the model in- and outflow tract, were identified in the segmented model. To get a realistic shape of the periphery of the valve annuli, a Visualization ToolKit (VTK, [28])-based program was created. Using the program, a sonographer identified the mitral annuli edges in thirteen 2D short axis (SA) B-mode views in ED, with each view rotated 15 degrees around the LV long axis. Using these points, the mitral annulus was estimated using a fitted spline with a smoothened Savitzky-Golay filter [29]. The same VTK-program was used to identify the aortic valve opening in a single three-chamber B-mode view in ES, which was fitted to a cylindrical shape. The identified valves were then projected onto the segmented surface mesh. All elements inside any of the valve regions were identified as belonging to either aortic (AV) or mitral valve (MV), respectively, with the rest of the elements identified as belonging to the endocardial wall. Due to difficulties of resolving 3D valve leaflet motion from TTE images, the valve regions were modelled as binary openings with the valves being either entirely open or entirely closed, depending on the cardiac phase.

4) Mesh Generation: From the initial surface mesh a finer mesh was obtained by subdividing elements, creating a surface mesh of in average 41 000±1000 nodes. Using this refined mesh, a tetrahedral volume mesh was generated with a maximum allowed side length of approximately 0.85 mm with introduced automatic refinement towards all model boundaries. The final volume mesh consisted of an average total of 380 000±30 000 nodes/2 000 000±140 000 cells. The chosen mesh density was based on prior preliminary mesh convergence studies on similar LV geometries (generated from endocardial segmentation), where mean outflow velocity and kinetic energy as a function of time was evaluated on meshes ranging from 40 000 to 1 250 000 nodes, with results indicating deviation below 2% when increasing mesh densities above 400 000 nodes. No numerical instabilities were observed in the performed mesh convergence studies. All meshes were created using ANSA 15.3 (BETA CAE Systems S.A., Greece). Temporal Hermite interpolation and mesh smoothing based on an elastic analogy was applied to enable an Arbitrary Lagrangian-Eulerian (ALE) CFD formulation [30], requiring mesh updates at each simulated time step.

5) Numerical Simulation: To describe the intraventricular blood flow, and to account for the temporal movement of the endocardial wall, an ALE formulation of the incompressible Navier-Stokes equations was used. This was obtained by replacing the convective velocity by the relative velocity with regards to the moving mesh. Denoting the fluid velocity $\boldsymbol{u}$, pressure p, kinematic viscosity ν, density ρ, and mesh velocity $\boldsymbol{m}$, this gives an expression on the form:

$$\frac{\partial u_i}{\partial t} + (u_j - m_j)\frac{\partial u_i}{\partial x_j} - \nu\frac{\partial^2 u_i}{\partial x_j^2} + \frac{1}{\rho}\frac{\partial p}{\partial x_i} = 0, \quad (x,t) \in \Omega\,(\mathrm{t}) \times I \tag{1a}$$

$$\frac{\partial u_i}{\partial x_i} = 0 \quad (x,t) \in \Omega(\mathrm{t}) \times I \tag{1b}$$

Using Einstein's notation of repeated indices corresponding to summation over spatial dimensions ($i, j = 1, 2, 3$), and with the spatial, time-dependent domain $\Omega\,(\mathrm{t}) \subset \mathbb{R}^3$ given over the time interval $I = (0, T)$. For all simulations, dynamic viscosity $\mu = 0.0027\ Pa \cdot s$ [31], [32] was set, with a blood density of $\rho = 1060\ kg/m^3$ (recalling $\nu = \mu/\rho$), with this neglecting non-Newtonian blood flow behaviour. Using the above ALE formulation, a time step of 1 ms was chosen, with a local coordinate map discretization accounting for mesh velocity variations as given in [30].

To retrieve the phases of the cardiac cycle, the volume of the segmented LV was extracted over time. Diastole was defined as spanning forward in time from the point of minimum LV volume (ED) to the point of maximum LV volume (ES). Systole was identified as spanning backward in time from ED to ES. With that, the isovolumetric phases of the cardiac cycles were not included in the model but incorporated into the diastolic and systolic phase, respectively. This was done partially based on the potential numerical instability in such phases due to the defined flow incompressibility, as well as on the phases small temporal extension [33], [34].

Dirichlet no-slip boundary conditions were imposed on the velocity at the endocardial wall by setting the flow velocity

equal to the prescribed velocity motion of the segmented wall. For the surface elements belonging to the MV during diastole, a flat inflow velocity profile perpendicular to the MV orifice was imposed with velocity magnitude derived from the mitral opening area and the change in LV volume, along with a defined zero relative static pressure. For the surface elements belonging to the AV during systole, only a defined zero relative pressure was prescribed, and outflow velocity was allowed to fluctuate according to the simulated output. With the valve pressure boundary conditions statically prescribed, any simulated pressure would be expressed as relative to any superimposed external pressure. Both valve regions were deemed to be either open with boundary conditions defined as above, or to be closed, during which the valve surface elements were considered as part of the wall, i.e. MV valve open during diastole, and AV valve open during systole.

For a given model, simulations were started at ED. To avoid influences from initiation conditions, four cardiac cycles were simulated, with results retrieved from the final one only. This choice was based on preliminary studies on temporal convergence, where the difference in regional mean flow velocities was seen to change less than 4% between the third and fourth simulated cardiac cycle in a given LV case.

CFD simulations were set up in a C++-environment, using the FEniCS framework and its high performance computing branch of the open source finite element library DOLFIN [35] along with the adaptive computational mechanics solver Unicorn [36]. The computations were parallelized using a hybrid OpenMP/MPI approach, with simulations carried out on a Cray XC40 system, with a total of 160 used cores.

6) Data Post-Processing: From the simulations, velocity and relative pressure fields were generated for the entire LV volume over a single cardiac cycle. With such, the proposed patient-specific pathway is not bounded to any particular post-processing procedure.

B. Robustness Evaluation

The robustness of the patient-specific CFD pathway was evaluated on 6 subjects: 3 with normal (LV ejection fraction (LVEF) $= 57 \pm 7\%$, cardiac output (CO) $= 3.9 \pm 0.2$ l/min, age: 28 ± 5) and 3 with reduced LV function (LVEF $= 28 \pm 9\%$, CO $= 3.4 \pm 1.8$ l/min, age: 57 ± 13). Apical 4DTTE images were acquired using a GE Healthcare Vivid E9 (4VD, 1.7MHz/3.3MHz, 34 - 54 fps).

Repeated models with different input variable perturbations were then generated. This included 4 repetitions of 4DTTE acquisitions by a single clinician, 4 repetitions of different clinicians performing the segmentation, 4 repetitions of segmentation from a single clinician, and 4 different MV and AV positioning from a single clinician, resulting in a total of 16 models/subject. For the repeated 4DTTE acquisitions, these were acquired during one imaging session with the sonographer instructed to reposition the probe between acquisitions. When a single clinician performed multiple segmentations or valve positioning, this was performed in a single-blinded manner with images from all subjects presented in random order.

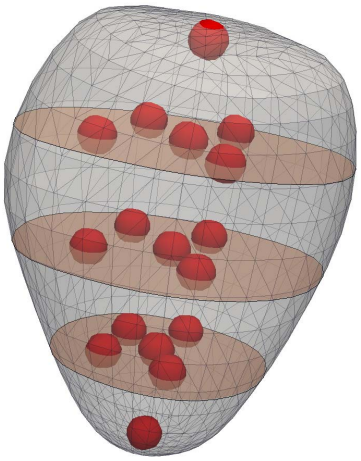

Fig. 2. Visualization of the 17 spherical regions within which mean velocities were derived for all models of the robustness evaluation. The spherical regions are visualized inside a coarsened surface mesh of the endocardium, together with three short-axis transverse cuts indicating where some spherical regions were positioned.

LV velocity fields were then simulated using the described pathway. To evaluate differences between repetitions, regional flow velocities were compared in each set of alternating input variable. For this, 17 spherical regions (radius $= 5$ mm, equalling $\sim$850 nodes) were seeded inside each simulated LV, positioned at: apex, centre-base, 3 regions equally spaced along the long axis connecting apex and MV centre, and, at each of these defined long-axis levels, 4 regions in the corresponding SA plane, each positioned half-way between long axis centre-line and endocardium, with ca. 90° between each region. Each spherical region was fixed to a specific set of surface nodes such that the chosen regions were following the overall movement of the LV over time. For visualization of the positioning of the spherical regions, see Figure 2.

For each spherical region, mean velocities were calculated for each subject. To evaluate the robustness, the coefficient of variation (CV) was calculated as

$$CV = \frac{\sigma}{\bar{u}} \tag{2}$$

with $\bar{u}$ and σ denoting mean velocity and standard deviation within a single perturbation set. To evaluate spatial differences, the results from the 17 spherical regions were projected onto 17-segment LV model [37]. CV variations were also evaluated at defined time points (peak systole (PS), E- and A-wave, ED, and ES, respectively), as well as for diastole and systole, respectively. As a mean robustness measure for the proposed pathway a time-averaged CV was computed for each input variable set, respectively. Patients with normal- and reduced LV function were additionally pooled to evaluate differences between the groups with regards to pathway robustness. This was statistically evaluated using a two-sample Kolmogorov-Smirnov test, whereas potential differences between LV segments were evaluated using a two-tailed t-test.

C. Validation Against In-Vivo Flow Measurements

A validation study was performed to compare the patient-specific CFD simulations and accuracy of the created pathway

against *in-vivo* ultrasound and PC-MRI flow measurements. For this, 4DTTE data were acquired from 100 subjects (47 women, 53 men, age: 62 ± 14): 50 with normal (LVEF = 58 ± 7%, CO = 3.6 ± 1.0 l/min, age: 61 ± 13) and 50 with reduced (LVEF = 41 ± 7%, CO = 3.4 ± 1.0 l/min, age: 63 ± 14) LV function, for which patient-specific CFD simulations were performed. All images were acquired using a GE Healthcare Vivid E9 (4VD, 1.7MHz/3.3MHz) with a framerate of 26 - 62 fps. The number of enrolled subjects was based on two-sampled t-test power calculations indicating a need for at least 47 subjects in order to detect an accuracy of 10% (assuming a significance level of $\alpha = 0.05, \beta = 0.1$, and using preliminary results for accuracy standard deviation).

With evaluation against both Doppler and PC-MRI, the validation study was performed in two steps: first the Doppler validation was performed to evaluate primarily the pre-processing of the presented pathway including segmentation and valve delineation, and second the PC-MRI validation was performed to evaluate the accuracy of the CFD simulations and the generated intraventricular flow field.

1) Ultrasound Validation: For all 100 subjects, spectral pulsed-wave (PW) Doppler was acquired during the 4DTTE at both MV and AV. The PW Doppler velocity was then extracted as the peak intensity in spectral signal, identified throughout the cardiac cycle. PW Doppler velocities were then compared with corresponding velocity components from the CFD simulations by extracting the average out/incoming velocities over the identified valve elements over time. Mean error and standard deviation were quantified at PS, E- and A-wave, ED and ES, respectively. A mean error for the entire cardiac cycle was also calculated for the subjects with normal and reduced LV function, respectively. Differences between the groups were statistically tested using a Kolmogorov-Smirnov test. With the corresponding CFD data at the valve openings governed by the volumetric LV change and the valve delineation in the chosen ALE-setup, this first step validation was performed to give information on the accuracy and validity of primarily the pre-processing of the pathway, including endocardial segmentation and valve delineation.

2) Magnetic Resonance Imaging Validation: Directly following the 4DTTE session, 6 subjects (4 with normal and 2 with reduced LVEF) were imaged in cardiac PC-MRI (3T, Philips Ingenia). To cover an extensive part of the LV and to evaluate flow components in different directions, a selection of 2D through-plane PC-MRI measurements were performed (short/long axis spatial resolution: $2.5\times2.5\times8$ mm^3/$1.9\times1.9\times8$ mm^3, temporal resolution: 53 ms) acquired in: 2-, 3-, and 4-chamber views, as well as in 4 SA views, equally distributed between mitral base and apex. For all planes, the mean through-plane velocity component, as well as the mean negative, and mean positive velocity component, was extracted using Segment v. 1.9 [38].

To compare PC-MRI with CFD simulations, the MRI images were fused with 4DTTE using a 3-chamber alignment algorithm [39]. Temporal alignment was achieved using ECG-data recorded both during 4DTTE and PC-MRI acquisition, with CFD data temporally registered to overlap with PC-MRI at ED and ES. Through-plane velocity component from all 2D planes (slice thickness = 8 mm) were identified in the simulated velocity fields, and subsequently compared to PC-MRI-based velocities. Differences in the form of mean error with standard deviation were quantified at PS, E- and A-wave, ED and ES, and for the entire cardiac cycle for subjects with normal- and reduced LV function, respectively. The differences between subjects with normal and reduced LV function were statistically evaluated using a Kolmogorov-Smirnov test. Complementary to the ultrasound validation, the PC-MRI evaluation, investigating correspondence between mean, negative, and positive velocity components, was performed to assess the accuracy of the simulated intraventricular flows.

III. Results

A. Patient-Specific CFD Simulations of the LV

Gathering all simulated patient-specific models for all outlined study parts, cardiac cycles spanning from 660 to 1400 ms were computed. With one simulated ms requiring approximately 60 seconds, this equalled a simulation time of around 16 hours per cardiac cycle. With pre-processing feasibly achieved within 15 minutes, and post-processing for visualization of velocity or relative pressure fields requiring around 30 minutes on a desktop computer, the overall turn-around time is approximately 17 hours. Note however that depending on the complexity of the post-processing, additional time might be required.

Figure 3 (previous page) shows the magnitude of the LV velocity field for one subject with normal and one with reduced LV function. For the subject with normal LV function, the simulated blood flow is characterized by a vortex forming in early diastole which deteriorates when interacting with the endocardial wall. During mid-diastole a relatively homogeneous flow with respective to velocity seems present, before a minor second vortex forms during atrial systole (surrounding the basal-most part of the red high-velocity jet entering through the open mitral valve in Figure 3(d)). The subject with reduced LV function showed similar behaviour with an even more distinct second vortex in atrial systole (surrounding the red high-velocity jet entering through the open mitral valve in Figure 3(h)), even though an overall LV dilatation with smaller EF seemed apparent.

B. Robustness Evaluation

Table 1 summarizes the main findings of the robustness evaluation, given for subjects with normal and reduced LV function. Additionally, Figure 4 (next page) gives the 17-segment bullseye plots for the spatial changes in CV.

For all perturbations for subjects with normal LV function, CV varied from 7% to 12% when averaging over the entire cardiac cycle. Smallest deviations were observed for perturbed valve position (CV $\approx$ 7% and 8% for AV and MV), whereas largest deviations were observed for repeated 4DTTE acquisitions (CV $\approx$ 12%). For all perturbations, CV seemed to decrease towards the basal part of the LV, with no pronounced difference in septal-lateral or inferior-anterior direction. However, no difference in the manual positioning of

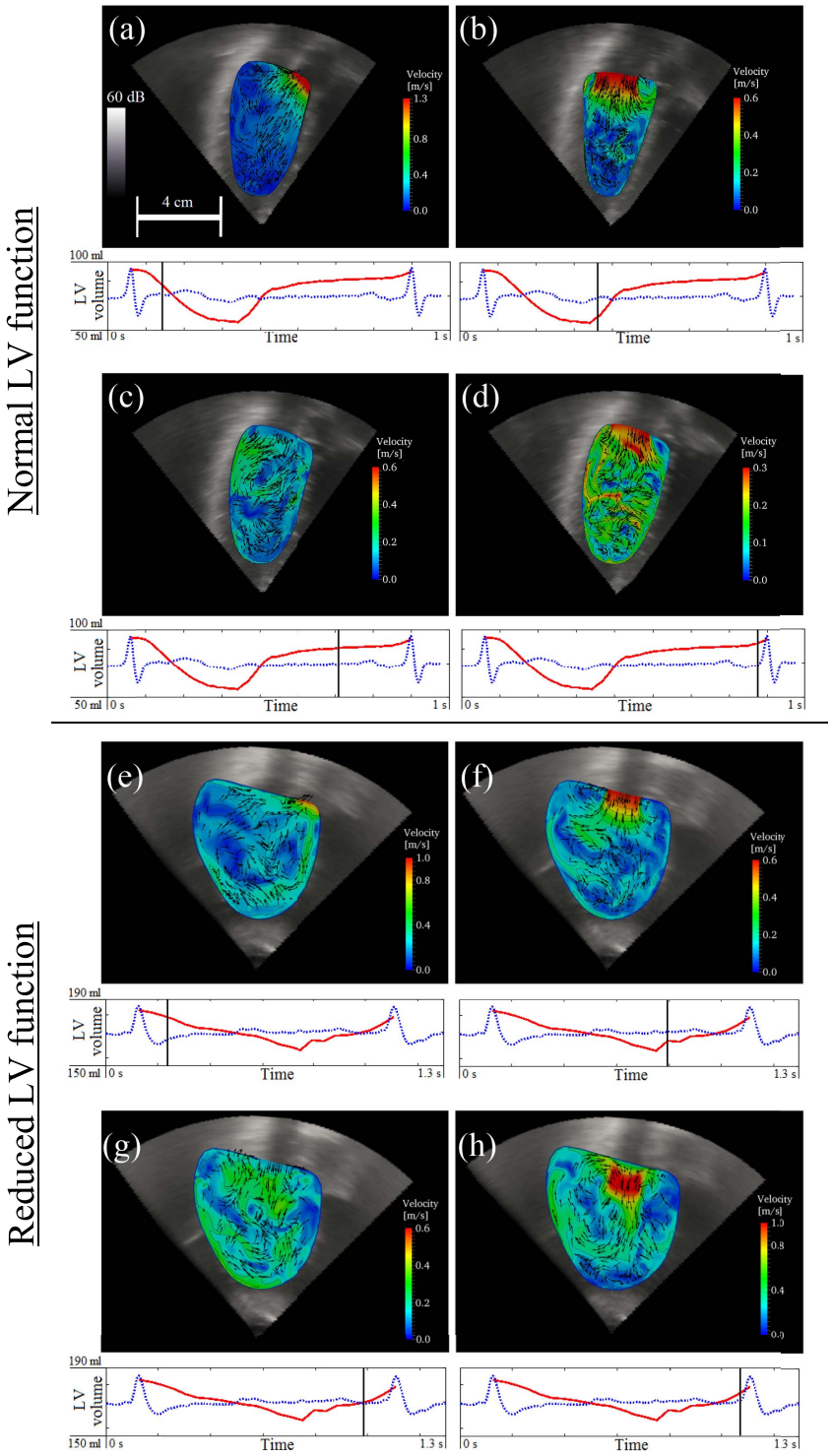

Fig. 3. Simulated left ventricular velocity fields for one subject with normal (top two rows, EF=57%) and one with reduced (bottom two rows, EF=22%) left ventricular function, provided in a 3 chamber view. Images are given at the onset of systole (a,e), onset of diastole (b,f), mid-diastole (c,g), and atrial systole (d,h)). The velocity fields are superimposed on a corresponding slice from the acquired 4D transthoracic echocardiography data. Note that metric and dynamic range scale valid for all images are given in (a).

apical or basal landmark was observed between different segmentations or different clinicians. Slightly higher CV was observed in systole (CV $\approx$ 9 – 11%), especially for apical regions, whereas the CV in diastole was relatively constant around 8 – 9% for all regions and all perturbations; however, for singular time points, peak E-wave generated slightly higher deviations than PS for basal segments (18 vs. 14%). For diastole, no major differences could be found between E- and A-wave, other than at the most basal segments where slightly higher deviations were found at the E-wave. Even though not

TABLE I

RESULTS FOR ROBUSTNESS EVALUATION GIVEN AS COEFFICIENT OF VARIATION [%] FOR ALL 17 DEFINED LEFT VENTRICULAR (LV) SEGMENTS (1: BASAL ANTERIOR, 2: BASAL ANTEROSEPTAL, 3: BASAL INFEROSEPTAL, 4: BASAL INFERIOR, 5: BASAL INFEROLATERAL, 6: BASAL ANTEROLATERAL, 7: MID ANTERIOR, 8: MID ANTEROSEPTAL, 9: MID INFEROSEPTAL, 10: MID INFERIOR, 11: MID INFEROLATERAL, 12: MID ANTEROLATERAL, 13: APICAL ANTERIOR, 14: APICAL SEPTAL, 15: APICAL INFERIOR, 16: APICAL LATERAL, 17: APEX). DATA IS GIVEN FOR SUBJECTS WITH NORMAL (a) AND REDUCED (b) LV FUNCTION, SPECIFIED FOR SYSTOLE (LEFT PART OF EACH COLUMN) AND DIASTOLE (RIGHT PART OF EACH COLUMN), AND FOR ALL MODEL PERTURBATIONS (AORTIC VALVE (AV), MITRAL VALVE (MV), SEGMENTATION, CLINICIAN, AND 4D TRANSTHORACIC ECHOCARDIOGRAPHY (4DTTE))

(a)	Coefficient of variation [%] – Normal LV function																													
	Basal segments												Mid segments												Apical segments					
Perturbation	1		2		3		4		5		6		7		8		9		10		11		12		13		14		15		16		17	
AV	6	7	7	7	7	7	7	6	7	8	7	8	7	8	7	8	7	9	7	9	8	8	8	7	8	8	6	7	6	9	7	9	7	8
MV	7	8	7	8	7	7	7	7	7	8	7	8	8	8	8	8	8	9	8	9	8	9	8	9	9	7	8	8	7	8	8	10	8	9
Segmentation	9	11	8	11	9	9	9	9	9	10	9	11	8	9	8	8	8	7	8	7	8	7	8	8	9	7	8	8	9	7	9	6	8	8
Clinician	8	9	8	8	8	7	7	6	8	7	8	9	10	9	10	9	10	9	9	9	10	7	11	7	11	9	10	8	11	7	12	8	13	12
4DTTE	10	10	10	10	10	10	10	8	10	9	10	10	12	9	12	10	11	11	10	11	9	10	10	9	14	12	14	9	11	11	13	12	13	10

(b)	Coefficient of variation [%] – Reduced LV function																													
	Basal segments												Mid segments												Apical segments					
Perturbation	1		2		3		4		5		6		7		8		9		10		11		12		13		14		15		16		17	
AV	4	4	5	6	6	7	6	5	6	5	5	4	7	9	7	8	6	7	6	6	6	7	7	8	6	8	6	8	7	12	7	9	6	6
MV	6	7	6	8	7	9	7	9	6	8	6	7	7	9	7	7	7	6	7	7	7	6	7	7	7	9	7	8	8	11	8	9	6	5
Segmentation	7	7	7	8	9	10	9	10	8	9	7	7	10	10	9	9	9	10	8	9	9	9	10	9	8	8	10	11	10	11	9	9	11	11
Clinician	8	7	8	8	9	10	9	10	9	9	9	7	11	13	9	9	9	10	9	10	9	11	10	12	10	9	9	12	11	11	10	9	13	11
4DTTE	10	9	9	9	10	9	10	10	10	10	10	10	12	11	10	10	10	9	11	9	11	11	11	10	12	13	12	13	11	9	10	10	11	7

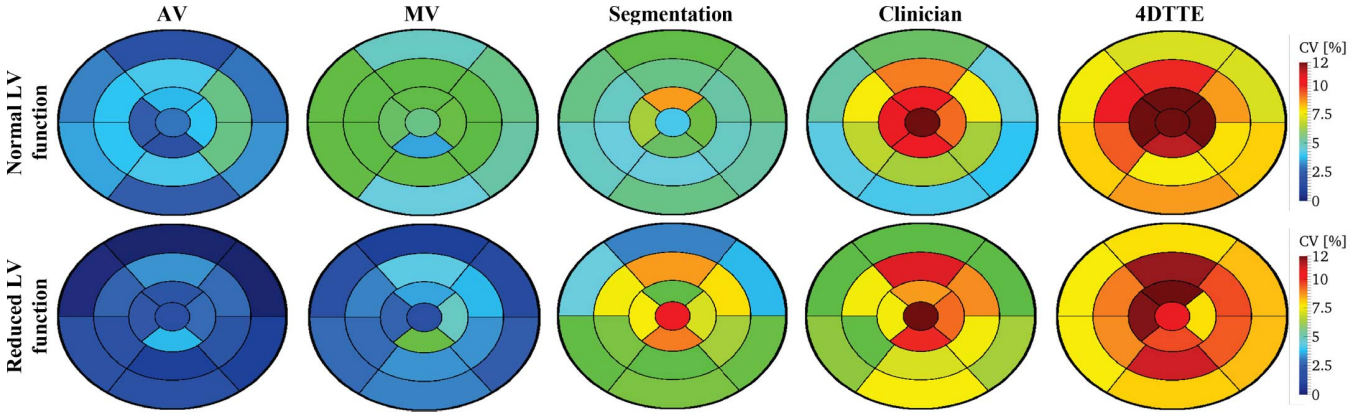

Fig. 4. 17-segment bullseye plots (left: septal, right: lateral, top: anterior, bottom: inferior) of coefficient of variation as a function of input variable perturbation (aortic valve, mitral valve, repeated segmentation, different clinicians segmenting, 4D transthoracic echocardiography acquisition) for subjects with normal (top row) and reduced (bottom row) LV functions (3 subjects each). The plots are given for a mean value over the entire cardiac cycle.

statistically significant, it is worth noting that for the subjects with normal LV function the basal inferior and lateral segments showed slightly higher intra-observer CV compared to inter-observer CV (in average 2 percentage points).

Similar trends in CV were observed for the subjects with reduced LV function, with CV varying between 6 and 10% for the entire cardiac cycle and all perturbations. Smallest deviations were observed for perturbed valve position (CV $\approx$ 6% and 7% for AV and MV, respectively), whereas repeated 4DTTE acquisitions showed highest deviations (CV $\approx$ 10%). However, the CV seemed spatially constant, with only slight increases in some apical anterior sections. No differences in the manual positioning of apical or basal landmark could be seen between model perturbations. Differences in CV between systole and diastole was not as pronounced for the subjects with reduced LV function as for the subjects with normal LV function, with slightly higher differences in systole and only a few apical sections showing inverted behavior. Singular time point deviations were slightly higher at peak E-wave with 16%, compared to PS with 12%. For the subjects with reduced LV function, inter-observer CV was consistently larger than intra-observer CV.

No statistically significant difference was found between subjects with normal and reduced LV function with regards to model robustness (Kolmogorov-Smirnov $D = 0.06$, with a rejection threshold for a 10% significance level at 0.24). This was valid even if evaluating systole or diastole separately.

C. Validation Against In-Vivo Flow Measurements

1) Ultrasound Validation: Table 2 shows the results from the comparison of CFD and PW Doppler. Additionally, Figure 5 gives an example of visual comparison between

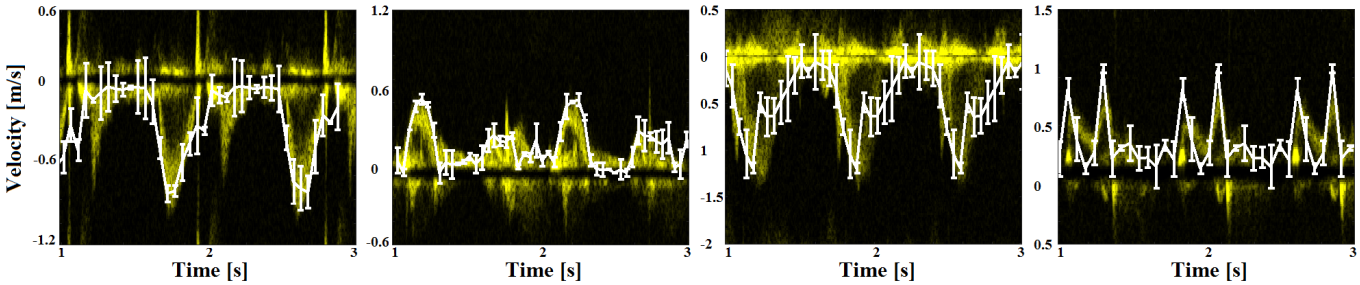

Fig. 5. Examples of PW Doppler for one subject with normal (a, b) and one with reduced (c,d) LV function, given for AV (a,c) and MV (b,d). PW Doppler is given by the yellow background intensity curves, with CFD values with standard deviation superimposed in white.

TABLE II

VALIDATION OF MEAN VELOCITIES INDICATING THE ACCURACY OF THE EVALUATED VOLUMETRIC CHANGE, GIVEN AGAINST PW DOPPLER AND MEAN FLOW PC-MRI WITH RESULTS GIVEN AS MEAN ERROR [cm/s] WITH STANDARD DEVIATION. DEFINED TEMPORAL DEVIATIONS ARE GIVEN AT PEAK SYSTOLE, E-WAVE, A-WAVE, END DIASTOLE, END SYSTOLE, AND FOR A TOTAL CARDIAC CYCLE AVERAGE, RESPECTIVELY. RESULTS ARE GIVEN FOR PATIENTS WITH NORMAL (a) AND REDUCED (b) LV FUNCTION, RESPECTIVELY

(a)		Mean velocity, mean error [cm/s] – Normal LV function					Total
		Peak systole	E-wave	A-wave	End diastole	End systole	
PWD US	MV	3.2 ± 2.4	6.2 ± 4.2	9.3 ± 5.4	3.3 ± 2.9	0.8 ± 0.7	7.2 ± 5.8
	AV	12 ± 10	2.6 ± 1.8	1.3 ± 0.9	0.9 ± 0.9	1.4 ± 1.0	4.8 ± 4.1
PC-MRI	SA base	5.3 ± 2.5	7.3 ± 6.2	2.9 ± 2.6	7.0 ± 5.5	6.9 ± 4.5	5.6 ± 3.7
	SA apical	5.6 ± 2.0	3.9 ± 3.1	1.2 ± 0.8	3.6 ± 3.2	3.3 ± 2.6	3.2 ± 1.3
	2ch	2.6 ± 2.6	3.4 ± 1.8	1.7 ± 1.0	1.3 ± 1.0	2.2 ± 2.1	2.1 ± 1.4
	3ch	3.1 ± 2.7	1.5 ± 1.3	1.8 ± 0.9	2.2 ± 1.0	2.1 ± 1.8	2.2 ± 1.0
	4ch	1.4 ± 0.9	5.4 ± 4.7	1.9 ± 1.9	1.3 ± 0.8	3.4 ± 3.6	2.5 ± 1.9

(b)		Mean velocity, mean error [cm/s] – Reduced LV function					Total
		Peak systole	E-wave	A-wave	End diastole	End systole	
PWD US	MV	2.7 ± 2.3	11 ± 6.6	16 ± 9.7	6.4 ± 4.2	3.3 ± 2.7	9.3 ± 6.9
	AV	14 ± 9.2	2.4 ± 1.8	2.1 ± 1.5	4.2 ± 3.3	5.8 ± 5.3	6.4 ± 3.2
PC-MRI	SA base	6.5 ± 4.8	10 ± 2.0	3.5 ± 0.8	12 ± 5.7	5.0 ± 1.4	8.6 ± 2.1
	SA apical	8.3 ± 4.7	8.2 ± 9.0	5.5 ± 4.2	5.3 ± 1.9	7.3 ± 2.8	6.9 ± 2.8
	2ch	4.5 ± 3.0	1.5 ± 1.4	3.5 ± 3.2	2.7 ± 1.2	4.3 ± 4.1	3.5 ± 1.5
	3ch	3.6 ± 1.3	1.8 ± 1.8	5.3 ± 5.0	0.7 ± 0.7	3.5 ± 2.4	3.7 ± 2.2
	4ch	3.8 ± 1.0	5.1 ± 2.0	2.3 ± 2.3	1.9 ± 1.5	1.3 ± 1.3	2.6 ± 0.9

CFD and PW Doppler. In general high agreement was seen between the two. For the subjects with normal LV function an absolute mean error of 7 ± 6 and 5 ± 4 cm/s for MV and AV was observed, amounting for a relative error below 7% for the entire cardiac cycle. During systole, maximum errors were observed at PS, with some subjects observing overestimated outflow velocities (singular case error up to 50%). For diastole, E-wave velocities were well captured with an error below 10%, whereas larger errors were observed at the A-wave (singular case errors up to 32%). For the subjects with reduced LV function mean errors of 9 ± 7 and 6 ± 5 cm/s for MV and AV were observed, amounting for a relative error below 10%. Compared to subjects with normal LV function, subjects with reduced LV function observed slightly higher errors at time points with lower absolute velocities (A-wave, ED, and ES) where especially valve regurgitations could not be properly captured by the simulation models. Again, in systole PS gave rise to highest errors (up to 62%), whereas the models were least successful in capturing A-wave velocities for diastole (singular deviation values of up to 38%).

For all subjects, the error against PW Doppler was normally distributed, however with a slight shift towards overestimation in simulations (−4 cm/s and −7 cm/s for subjects with normal and reduced LV function, respectively). The shift could however not be statistically determined, neither could any significant distinction be made between PW Doppler and CFD comparing subjects with normal and reduced LV function (maximum Kolmogorov-Smirnov $D = 0.18$, with a rejection threshold for a 10% significance level at 0.24).

2) Magnetic Resonance Imaging Validation: For the evaluation against PC-MRI measurements, ejection fraction (EF) and cardiac output (CO) was measured as 58% vs 53% and 4.4 l/min vs 4.1 l/min for the subjects with normal LV function, and 40% vs 45%, and 3.1 l/min vs 3.4 l/min for the subjects with reduced LV function, with values given from 4DTTE and MRI, respectively.

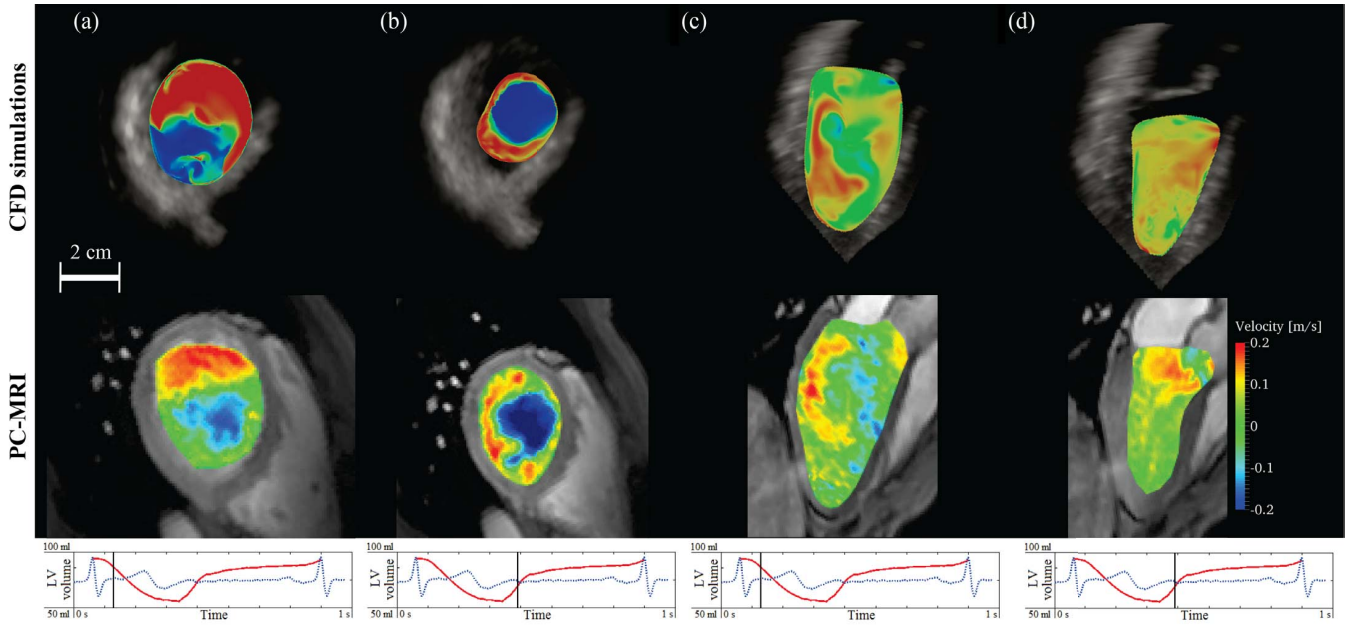

Fig. 6. Mid-SA plane (a,b) and 3-chamber view (c,d) of CFD simulated through-plane velocity (top row) against measured through-plane PC-MRI velocity (bottom row). Results are given at the onset of systole (a,c) and diastole (b,d), respectively, for one subject with normal left ventricular function. The colourbar is valid for all images. Note that the subject shown above is different from the ones given in Figure 3.

Figure 6 provides the through-plane velocity component of the mid-SA plane as well as for the 3-chamber view, from CFD and PC-MRI for one of the evaluated subjects with normal LV function. Overall, some flow features seem to be captured by the simulations, with areas of major in- and outgoing flow being positioned in similar regions as the PC-MRI; a matter most clearly visible in the shown SA planes (Figure 6 (a) and (c)), with similar changes in lateral-septal direction. For regions of lower absolute velocities the detailed flow features seen in simulations could not be as distinctly identified in the corresponding PC-MRI, as seen in the given flow features seen in simulations could not be as distinctly 3-chamber view example (Figure 6 (b) and (d)), even though a similar vortex-like structure can be seen at the lateral wall in early systole.

Figure 7 (previous page) gives an excerpt of overlaid PC-MRI and CFD averaged through-plane velocity component over time for one subject with normal and reduced LV function, respectively. The data is given for both mean velocity, as well as mean positive, and mean negative velocity separately.

The results for the mean error between simulations and PC-MRI are given in Table 2 and Table 3. In Table 2, a comparison of mean velocity component is given, describing primarily the accuracy of the wall motion and endocardial segmentation. In Table 3, a comparison of PC-MRI and simulated positive and negative velocity components is given, in order to evaluate the accuracy of the simulated intraventricular flow. Generally, both analyses show high correspondence between PC-MRI and CFD simulations. In the case of mean flow (Table 2), the subjects with normal LV function seem to be captured with slightly higher accuracy, even though some fluctuations seem apparent in CFD. For the subjects with normal LV function, a mean velocity error between 2.1 cm/s – 5.6 cm/s was observed for the entire LV, with largest error seen for the most basal SA and the 4-chamber view. No significant temporal differences in mean flow error could be observed for different time points, and in general the subjects with normal LV function had a relative error of below 6% in mean velocities. For the subjects with reduced LV function similar error values were seen with an overall mean velocity error of 2.6 cm/s – 8.6 cm/s for the entire LV, with the apical SA view showing highest deviation. In general, a relative error of below 8% in mean velocity was observed for this subset of subjects.

For the PC-MRI comparison of mean positive and mean negative velocities (Table 3) the subjects with normal LV function had a mean positive velocity error between 5.1 – 11 cm/s and a mean negative velocity error between 3.9 – 9.8 cm/s for the entire LV. For both velocity types, the most basal SA plane showed highest errors, especially for mean positive velocities where deviations of up to 35 cm/s was observed in singular time points (peak E-wave for one of the subjects). In general, the subjects with normal LV function had a relative error in mean positive and mean negative velocity of below 11% and 8%, respectively. For the subjects with reduced LV function, the mean positive velocity error was between 2.2 – 6.6 cm/s, and the mean negative velocity error was between 2.4 – 7.4 cm/s for the entire LV. For both velocity types, the most basal SA plane showed highest mean deviations, however one subject had mean negative velocity errors of up to 25 cm/s in an apical SA plane at peak systole. However, no significant changes could be observed over time for neither subjects with reduced nor subjects with normal

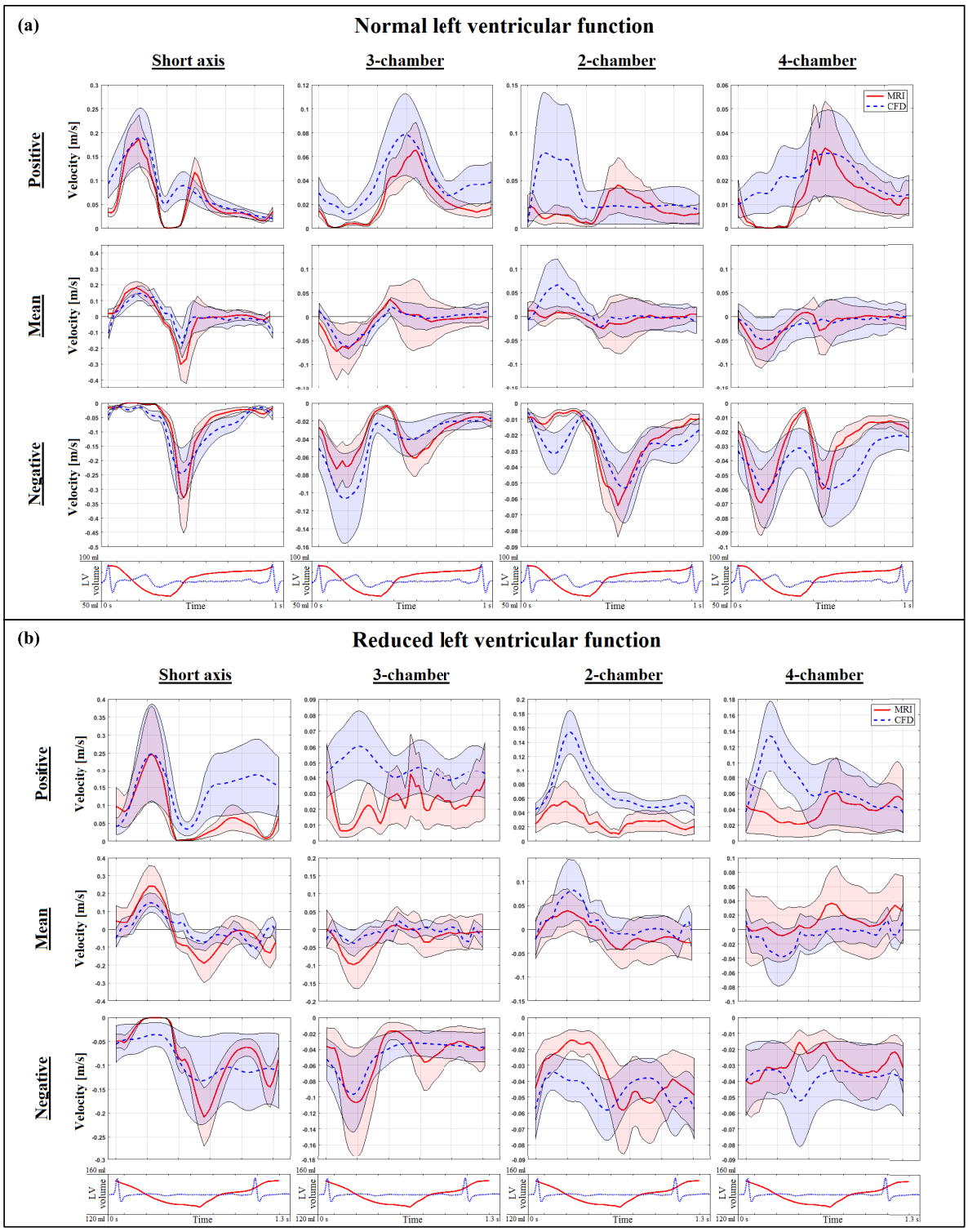

Fig. 7. Example of mean positive, mean total, and mean negative through-plane velocity component over time for computational fluid dynamics (CFD) simulations (CFD, blue dashed line) against corresponding PC-MRI (red solid line) with corresponding standard deviation. Results are given for one subject with normal (a) and one with reduced (b) LV function. Data is given for mid-short-axis (1st column), 3-chambers (2nd column), 2-chamber (3rd column), and 4-chamber (4th column) views, respectively. Note that the velocity axes are different between different planes and velocity components.

LV function. The subjects with reduced LV function had a relative error in mean positive and mean negative velocity of below 9 and 6%, respectively.

For all evaluated mean, positive, and negative velocities, the Kolmogorov-Smirnov evaluation did not reveal any significant difference in error between the two subject groups for any of the evaluated planes (maximum Kolmogorov-Smirnov $D = 0.06$, with a rejection threshold of 1.06 for a 10% significance level). The error against PC-MRI was normally distributed for all velocity types, with a slight but not

TABLE III
VALIDATION OF MEAN POSITIVE (a,c) AND MEAN NEGATIVE (b,d) VELOCITIES INDICATING THE ACCURACY OF THE SIMULATED INTRAVENTRICULAR VELOCITY FIELD AGAINST REFERENCE PC-MRI, GIVEN AS A MEAN ERROR [cm/s] WITH STANDARD DEVIATION. RESULTS ARE GIVEN FOR SUBJECTS WITH NORMAL (a,b) AND REDUCED (c,d) LV FUNCTION, RESPECTIVELY, AND PROVIDED AT PEAK SYSTOLE, E-WAVE, A-WAVE, END DIASTOLE, END SYSTOLE, AND FOR A TOTAL CARDIAC CYCLE AVERAGE, RESPECTIVELY

(a)		Mean positive velocity, mean error [cm/s] – Normal LV function					Total
		Peak systole	E-wave	A-wave	End diastole	End systole	
PC-MRI	SA base	6.9 ± 4.4	19.3 ± 15	7.7 ± 6.9	6.7 ± 3.1	15.9 ± 6.4	11.0 ± 8.1
	SA apical	5.7 ± 3.1	8.0 ± 5.3	8.4 ± 5.8	8.7 ± 5.2	7.0 ± 4.5	7.6 ± 3.3
	2ch	7.7 ± 2.5	3.3 ± 1.0	4.2 ± 0.5	5.8 ± 1.5	3.7 ± 1.6	5.4 ± 2.4
	3ch	8.5 ± 4.9	3.0 ± 1.2	4.1 ± 0.8	5.7 ± 1.2	2.1 ± 1.2	5.1 ± 3.3
	4ch	9.3 ± 4.5	5.5 ± 1.5	4.6 ± 1.6	5.9 ± 2.8	4.7 ± 2.3	6.9 ± 3.2
(b)		Mean negative velocity, mean error [cm/s] – Normal LV function					Total
		Peak systole	E-wave	A-wave	End diastole	End systole	
PC-MRI	SA base	8.7 ± 4.6	9.6 ± 6.5	5.1 ± 3.4	5.5 ± 3.9	7.0 ± 2.7	9.8 ± 4.6
	SA apical	6.2 ± 6.2	4.5 ± 2.6	4.5 ± 1.8	5.6 ± 4.5	5.1 ± 3.5	5.4 ± 2.8
	2ch	2.8 ± 1.6	5.3 ± 2.0	3.6 ± 1.8	3.4 ± 1.6	5.1 ± 2.3	3.9 ± 1.8
	3ch	4.2 ± 1.6	5.7 ± 1.1	5.4 ± 1.6	4.4 ± 1.6	6.1 ± 0.8	4.8 ± 1.5
	4ch	4.3 ± 4.2	6.0 ± 3.7	5.7 ± 2.4	5.3 ± 2.4	5.6 ± 3.1	5.5 ± 2.6

(c)		Mean positive velocity, mean error [cm/s] – Reduced LV function					Total
		Peak systole	E-wave	A-wave	End diastole	End systole	
PC-MRI	SA base	11.5 ± 3.8	9.1 ± 2.6	3.8 ± 1.2	7.1 ± 2.8	8.4 ± 2.3	6.6 ± 3.9
	SA apical	6.0 ± 1.1	3.1 ± 1.6	4.7 ± 3.4	6.5 ± 3.0	5.2 ± 1.1	4.6 ± 2.6
	2ch	7.4 ± 3.8	2.8 ± 3.0	3.5 ± 3.2	5.2 ± 0.9	2.8 ± 3.1	4.6 ± 2.0
	3ch	4.4 ± 3.5	1.8 ± 0.8	1.5 ± 1.3	2.8 ± 2.2	2.9 ± 2.7	3.3 ± 1.8
	4ch	4.0 ± 5.6	0.9 ± 0.3	1.1 ± 1.1	0.9 ± 2.2	2.4 ± 0.7	2.2 ± 2.2
(d)		Mean negative velocity, mean error [cm/s] – Reduced LV function					Total
		Peak systole	E-wave	A-wave	End diastole	End systole	
PC-MRI	SA base	8.8 ± 3.7	5.7 ± 4.2	6.6 ± 4.9	1.8 ± 1.6	7.7 ± 4.0	7.4 ± 5.0
	SA apical	15.4 ± 10.6	6.8 ± 5.8	5.8 ± 2.6	3.5 ± 2.8	7.8 ± 4.7	4.6 ± 3.6
	2ch	2.6 ± 1.1	1.6 ± 3.1	0.2 ± 0.2	1.6 ± 1.6	2.9 ± 2.0	2.4 ± 1.3
	3ch	4.4 ± 4.1	1.8 ± 0.7	3.0 ± 2.8	2.5 ± 2.2	3.7 ± 0.7	3.0 ± 1.9
	4ch	4.5 ± 3.3	2.7 ± 1.8	2.3 ± 2.1	2.1 ± 2.0	3.1 ± 1.6	2.7 ± 2.5

significant shift towards overestimations in CFD (−3, −2, and −3 cm/s for mean, positive, and negative velocity).

IV. DISCUSSION

In this paper, a TTE-based pathway for patient-specific CFD simulations of the LV has been presented. An evaluation of pathway robustness has been performed, together with a validation against *in-vivo* flow measurements. A main advantage of the presented pathway lies in that all necessary boundary conditions can be derived from routinely acquired 4DTTE images. With echocardiography being the primary imaging modality for diagnosing cardiac patients, the pathway could easily be connected to clinical studies, and offers a novel approach to studying detailed intraventricular flow. Additionally, with most previous work on cardiac CFD primarily validated qualitatively or on single subjects [12]–[14], the study includes a validation on numerous subjects of both normal and reduced LV function, respectively, indicating a high agreement to both ultrasound and MRI-based flow measurements.

A. Patient-Specific CFD Simulations of the LV

With the presented pathway being patient-specific each simulation will be inherently unique. However, general flow patterns can be observed, as in Figure 3. An initial symmetrical ring vortex develops in early diastole, which deteriorates asymmetrically with the vortex positioned laterally off centre in the LV. During systole, a more constant velocity field is seen. All these findings correspond well to what has been reported in literature from both simulated [12], [13], as well as clinically measured velocity fields [37], [40]. The reduction in flow circulation and vortex strength apparent in the provided example from a subject with reduced LV function is also in agreement with previous findings [41], [42].

B. Robustness Evaluation

An overall model deviation of around 10% was seen for all evaluated subjects and tested input variable perturbations. For all perturbations, CV increased towards apex, even though no differences could be seen in the positioning variation of apex or base landmark. Instead this behaviour could potentially

be explained by: 1) error propagation from areas of main in/outflow (base) to areas of circulating flow (apex), or 2) the fact that apical regions experience predominantly low velocity flows, where small absolute deviations may give rise to larger relative deviations (apical circulatory flow is supported by e.g. intraventricular pressure differences between apex and base [43], or by a decrease in pulsatile flow [42]). Note that larger apical deviations seem apparent even for perturbed valve positions where there are no volumetric differences between models. The effect of changing MV position has been studied previously [44], where 5-15% velocity changes were reported upon changing inflow direction, similar to our findings of around 10%. Apart from this, no major evaluations have to the best of our knowledge been performed on the robustness of cardiac CFD models. Mihalef *et al.* [16] mentioned the inter-user variability in valve delineation, however did not expand on its effect on flow. Others have studied the effect different of boundary conditions at the MV, indicating that vortex skewing might occur when changing MV size or the region of imposed pressure prescription [45], [46].

C. Validation Against In-Vivo Flow Measurements

Generally, results indicate a strong agreement between simulations and ultrasound and PC-MRI measurements, with the reported relative error being on average below 10% for the evaluated 100 subjects.

The evaluation against PW Doppler was primarily performed to evaluate the accuracy of the pathway pre-processing steps, including endocardial segmentation and valve delineation. The reason to this lies in the setup of the simulation: with a chosen ALE-approach and an incompressible flow description, the inflow and outflow is exclusively governed by the volumetric change together with the size of the delineated valves (following the direct relation between flow, velocity and valve area, a delineation error of 10% would result in a 10% velocity error, and similarly would a 10% volumetric error result in a 10% velocity error at in- or outflow). For the intraventricular flow, any incorrect deviation within pre-processing would however most likely be highly detrimental to the overall simulated velocity fields, wherefore this initial validation is still of importance for the simulated flows. With all of this in mind, the errors of below 10% indicated both well-delineated AV and MV-regions and well-segmented endocardial borders, meaning that relatively accurate model definition and input variables were fed into the numerical setup and solution of the intraventricular blood flow. For the PW Doppler validation, larger deviations of over 50% were found at discrete temporal positions for some subjects with decreased LV function. This could be an indication that valve delineation might be an issue, potentially following reduced image quality in diseased subjects. Additionally, with the CFD models only covering the LV, any flow regurgitation would be neglected as long as it would not give rise to detectable volumetric changes. With valve regurgitation being more prevalent in subjects with reduced LV function [47], the potential for larger deviations at the valve positions would thus be more pronounced.

For the second part of the validation the CFD simulations were evaluated against PC-MRI, both with regards to mean velocity as well as separated in mean positive and mean negative velocity, respectively. Similar to the PW Doppler assessment, the evaluation of mean PC-MRI velocity primarily provided data regarding the quality of the tracked volumetric change through the defined LV plane. With such, the reported relative error of below 10% further supports the PW Doppler results indicating accurate segmentation and valve delineation. For subjects with normal LV function the most basal SA-plane showed largest differences between PC-MRI and CFD, whereas for subjects with reduced LV function the most apical SA-plane experienced the largest differences. However, none of these changes seemed to differ significantly from any other LV planes, wherefore the indicated accuracy level seemed valid for the entire LV volume.

The evaluation of mean negative and mean positive velocities in PC-MRI and CFD, respectively, resulted in a more direct validation of the simulated LV flow. With such, the mean positive and mean negative velocity errors of below 11 and 8%, respectively, indicates that accurate measures of intraventricular flow parameters can be obtained using the presented simulation pathway. It seemed that slightly larger deviations were seen at temporal positions with predominantly higher velocities (such as PS or E-wave) however the differences could not be proven statistically significant. For subjects with normal LV function slightly larger mean positive and mean negative velocity errors were seen in the basal SA-plane, whereas higher errors were seen in more apical SA-plane for subjects with reduced LV function. As discussed before, higher apical errors may be explained by pronounced circulatory flow observed in such regions and for such subjects [41]. However, the reported error did not seem to be significantly different from any other plane, and effects from incorrect valve delineation, temporal smoothing in PC-MRI, heart rate variations, or co-registration misalignments between 4DTTE and MRI could have had an equally influential effect on the reported errors.

As mentioned previously, only a few examples of echo-based patient-specific CFD models exist in literature. TEE approaches have been presented [20]–[21] but would, in comparison to the performed study, require imaging beyond what is routinely acquired in primary cardiac care. Voigt et al even expanded their TEE approach with quantitative validation comparing simulations with Doppler at the MV and AV but with their evaluation performed on a subset of 3 subjects, the present work represents a significantly enlarged validation. A few recent TTE-based approaches exist [22], [41] but comparing to the current work, there is a lack of output validation against *in-vivo* measurements. In general, *in-vivo* validation is uncommon and only very few proposed models have attempted such. For these, mainly flows at MV or AV have been evaluated, where errors of 10 cm/s [14] or 10-20% [13] have been reported against PC-MRI, or around 10% when evaluating cardiac-mimicking *in-vitro* phantoms [23], [24]: all similar to the range reported in our work. When comparing to all aforementioned models, the current study represents a novel work by its validation against multimodal *in-vivo* flow measurements, performed at multiple

positions in the LV, on several subjects with both normal and reduced LV function.

Despite the reported correspondence to *in-vivo* measurements, a few limitations are worth pointing out. First and foremost, the pathway does not include any valve leaflets. Their effect on intraventricular flow has been widely discussed and even though it has been argued that they merely orient themselves into the main flow [14], other studies have indicated their role in vortex development [48], positioning [21], and apical washout [49]. The lack of leaflets represents the main drawback of the current study, even though the valve delineation allows for a physiological opening shape. The validation also indicates that accurate flows can be obtained with the current pathway. There is however a clear potential of including valve anatomy with echocardiography possibly able to resolve such [50]. For the valve openings, the defined boundary conditions should also be mentioned, where previous studies have indicated that the choice of such might influence the estimation of the intraventricular flow fields [13], [45]. Even though the validation study indicates a defined correspondence between simulated and measured flows using the presented model pathway, the results on negative and positive flow components indicate that velocities closer to the valves (at more basal short-axis planes) have higher deviations than apical ones, with such basal flows having a potentially higher influence by the defined valve boundary conditions. If attempting future work on regional flow behaviour, additional studies on the sensitivity of the presented pathway against different valve boundary conditions could therefore be attempted. Apart from these mentioned boundary conditions and the influence of the geometry of the intraventricular valves, other anatomical features have also shown to impact LV blood flow such as e.g. papillary muscles [15] or ventricular trabeculation [51], wherefore such may be included in future model developments. Also, adjusting the numerical setup to incorporate a priori flow information from patient-specific Doppler measurements could be explored in the future.

With regards to model limitations, a slight drawback lies in the assumption of the intraventricular blood flow being purely Newtonian. In general, this assumption has been made following the predominant high shear rate flow inside the ventricle originating from high velocities and large geometries, as has been done by other similar numerical studies [12]–[16], even though a quantitative shear rate analysis will depend on the choice of hemorheological model. A recent study on the effect of different hemorheological models on LV flow has indicated changes in LV wall shear stresses, but the same study has also shown that deviations in regional velocity magnitude between different hemorheological models were below those reported in the current validation study [52]. This indicates that the presented model pathway may still capture accurate general flow behaviour. However, if attempting to study highly regional flows, or flows of low shear stresses such as stagnation or leaflet circulation, non-Newtonian blood flow behaviour may have to be taken into account, together with other model assumptions such as the influence of valve leaflet motion or endocardial trabeculation.

For the robustness evaluation, a detailed assessment of flow deviations as a function of image quality (by modifying endocardial contrast or acquired frame rate) could be attempted. In general, even though all clinical images were acquired with constant transmission and receiver setting, variations in acquired field-of-view and frame rate (hence effecting lateral spatial and temporal resolution) could be present. Even though a previous study has indicated variations of 7% for a resolution of 2 mm and 30 ms [22] being below the variation reported for the evaluated perturbations of the present study, the detailed effect of deteriorating frame rate and image quality could be explored in future studies. Additionally, uncertainty quantification schemes could be proposed to disentangle the numerical influence of mesh smoothing or penalization on the simulated output. Also, the clinical implications of a 10% deviation remain to be investigated, as does it remain to be investigated what influence the chosen regional sphere radius has on the evaluated pathway robustness. Lastly, the intra-observer robustness of the pathway when 4DTTE acquisitions are repeated days apart is still to be determined, even though studies on repeated 4DTTE indicates high repeatability with respect to derived volumetric data [53].

Another important limitation is the use of 2D flows to evaluate the simulated 4D flow fields. Also, averaged instead of regional velocity are compared, with measurements performed at slightly different times. Similarly, the through-plane slice thickness of 8 mm might limit the method's ability to capture low velocity circulatory flow components, even though results indicate non-zero velocity components throughout the cardiac cycle. A potential advancement for all of this would be a comparison with 4D flow MRI. As of now, the performed validation only describes global flow metrics, and it remains to be seen how well the presented pathway captures highly regional flows. However, assessing differences in regional flows might be challenging, and it could be difficult to determine whether potential disagreements spur from actual modelling or from co-registration misalignment, phase offsets, or from difference in temporal and spatial resolution. With that in mind, good correspondence has been shown between 2D CINE PC-MRI and 4D flow MRI [12], and with the former being the more clinically established method, such a comparison represents a practical evaluation method. Future attempts using 4D flow MRI could very well be made, where global flow metrics such as kinetic energy and flow component differences could be compared.

With the presented TTE-based pathway for patient-specific CFD modelling of the LV proven robust and with a validated accuracy level, there is a potential for more clinically oriented future studies. Using CFD modelling, the possible relationship between 3D blood flow and cardiovascular pathologies could be investigated in-detail. Similarly, simulations could be used to evaluate the consequences of future surgical intervention, or to study how blood flow motion can be quantified in a clinically relevant manner.

V. Conclusion

This paper has presented a novel TTE-based pathway for patient-specific CFD modelling of the LV. A performed

robustness evaluation has quantified the sensitivity of the simulation pathway, showing a deviation of below 12% when varying input parameters such as image acquisition or evaluating clinician. Additionally, the accuracy of the pathway has also been quantified, showing average errors of below 11% between simulations and clinically acquired *in-vivo* flow measurements. With both robustness evaluation and validation study performed on subjects with normal and reduced LV function, respectively, there is a clear potential for the continued use of the simulation models in clinical evaluations. In general, with patient-specific models enabling the detailed study of isolated flow phenomena in direct relation to defined pathologies, the presented pathway may serve as a valuable tool for future clinical investigations of 3D blood flow motion.

Acknowledgment

Computations were performed on resources provided by the Swedish National Infrastructure for Computing at the PDC Centre for High Performance Computing. The authors would like to thank the Jonasson Centre for Medical Imaging for providing the imaging equipment, as well as clinical staff at the heart clinics at Karolinska University Hospital in Huddinge and Danderyd for assisting during imaging.

References

[1] P. J. Kilner, G.-Z. Yang, A. J. Wilkes, R. H. Mohiaddin, D. N. Firmin, and M. H. Yacoub, "Asymmetric redirection of flow through the heart," *Nature*, vol. 404, pp. 759–761, Feb. 2000.

[2] S. Beppu *et al.*, "Abnormal blood pathways in left ventricular cavity in acute myocardial infarction. Experimental observations with special reference to regional wall motion abnormality and hemostasis," *Circulation*, vol. 78, no. 1, pp. 157–164, 1988.

[3] A. F. Bolger *et al.*, "Transit of blood flow through the human left ventricle mapped by cardiovascular magnetic resonance," *J. Cardiovascular Magn. Reson.*, vol. 9, no. 5, pp. 741–747, 2007.

[4] G. Pedrizzetti, G. L. Canna, O. Alfieri, and G. Tonti, "The vortex—An early predictor of cardiovascular outcome?" *Nature Rev. Cardiol.*, vol. 11, no. 9, pp. 545–553, 2014.

[5] T. Asaka, J. Yoshikawa, K. Yoshida, K. Koizumi, F. Okumachi, and K. Yanagihara, "Sensitivity and specificity of real-time two-dimensional doppler flow imagnig-system in the detection of valvular regurgitation," *Circulation*, vol. 70, no. 38, p. 38, 1984.

[6] L. Hatle, B. Angelsen, and A. Tromsdal, "Non-invasive assessment of aortic stenosis by Doppler ultrasound," *Heart*, vol. 43, no. 3, pp. 284–292, 1980.

[7] J. Bercoff *et al.*, "Ultrafast compound Doppler imaging: Providing full blood flow characterization," *IEEE Trans. Ultrason., Ferroelect., Freq. Control*, vol. 58, no. 1, pp. 134–147, Jan. 2011.

[8] J. A. Jensen, S. I. Nikolov, K. L. Gammelmark, and M. H. Pedersen, "Synthetic aperture ultrasound imaging," *Ultrasonics*, vol. 44, pp. e5–e15, Dec. 2006.

[9] A. Kheradvar *et al.*, "Echocardiographic particle image velocimetry: A novel technique for quantification of left ventricular blood vorticity pattern," *J. Amer. Soc. Echocardiograph.*, vol. 23, no. 1, pp. 86–94, 2010.

[10] P. D. Gatehouse *et al.*, "Applications of phase-contrast flow and velocity imaging in cardiovascular MRI," *Eur. Radiol.*, vol. 15, no. 10, pp. 2172–2184, 2005.

[11] Z. Stankovic, B. D. Allen, J. Garcia, K. B. Jarvis, and M. Markl, "4D flow imaging with MRI," *Cardiovascular Diagnosis Therapy*, vol. 4, no. 2, pp. 173–192, 2014.

[12] Q. Long, R. Merrifield, X. Y. Xu, P. Kilner, D. N. Firmin, and G.-Z. Yang, "Subject-specific computational simulation of left ventricular flow based on magnetic resonance imaging," *Proc. Inst. Mech. Eng., H, J. Eng. Med.*, vol. 222, no. 4, pp. 475–485, 2008.

[13] T. Schenkel, M. Malve, M. Reik, M. Markl, B. Jung, and H. Oertel, "MRI-based CFD analysis of flow in a human left ventricle: Methodology and application to a healthy heart," *Ann. Biomed. Eng.*, vol. 37, no. 3, pp. 503–515, 2009.

[14] N. R. Saber *et al.*, "Progress towards patient-specific computational flow modeling of the left heart via combination of magnetic resonance imaging with computational fluid dynamics," *Ann. Biomed. Eng.*, vol. 31, no. 1, pp. 42–52, 2003.

[15] J. Lantz, L. Henriksson, A. Persson, M. Karlsson, and T. Ebbers, "Patient-specific simulation of cardiac blood flow from high-resolution computed tomography," *J. Biomech. Eng.*, vol. 138, no. 12, p. 121004, 2016.

[16] V. Mihalef *et al.*, "Patient-specific modelling of whole heart anatomy, dynamics and haemodynamics from four-dimensional cardiac CT images," *Interface Focus*, vol. 1, no. 3, pp. 286–296, 2011.

[17] I. Borazjani, J. Westerdale, E. M. McMahon, P. K. Rajaraman, J. J. Heys, and M. Belohlavek, "Left ventricular flow analysis: Recent advances in numerical methods and applications in cardiac ultrasound," *Comput. Math. Methods Med.*, vol. 2013, Apr. 2013, Art. no. 395081.

[18] M. Cikes, L. Tong, G. R. Sutherland, and J. D'hooge, "Ultrafast cardiac ultrasound imaging: Technical principles, applications, and clinical benefits," *JACC, Cardiovascular Imag.*, vol. 7, no. 8, pp. 812–823, 2014.

[19] R. Mittal *et al.*, "Computational modeling of cardiac hemodynamics: Current status and future outlook," *J. Comput. Phys.*, vol. 305, pp. 1065–1082, Jan. 2016.

[20] I. Voigt *et al.*, "Patient-specific model of left heart anatomy, dynamics and hemodynamics from 4D TEE: A first validation study," in *Functional Imaging and Modeling of the Heart*. Berlin, Germany: Springer, 2011, pp. 341–349.

[21] A. Bavo *et al.*, "Patient-specific CFD simulation of intraventricular haemodynamics based on 3D ultrasound imaging," *Biomed. Eng. OnLine*, vol. 15, no. 1, p. 107, 2016.

[22] A. de Vecchi *et al.*, "A novel methodology for personalized simulations of ventricular hemodynamics from noninvasive imaging data," *Comput. Med. Imag. Graph.*, vol. 51, pp. 20–31, Jul. 2016.

[23] S. Krittian, T. Schenkel, U. Janoske, and H. Oertel, "Partitioned fluid–solid coupling for cardiovascular blood flow: Validation study of pressure-driven fluid-domain deformation," *Ann. Biomed. Eng.*, vol. 38, no. 8, pp. 2676–2689, 2010.

[24] V. Vedula, S. Fortini, J.-H. Seo, G. Querzoli, and R. Mittal, "Computational modeling and validation of intraventricular flow in a simple model of the left ventricle," *Theor. Comput. Fluid Dyn.*, vol. 28, pp. 589–604, Dec. 2014.

[25] D. Larsson *et al.*, "Patient-specific flow simulation of the left ventricle from 4D echocardiography—Feasibility and robustness evaluation," in *Proc. IEEE Int. Ultrason. Symp.*, Taipei, Taiwan, Oct. 2015, pp. 1–4.

[26] D. Larsson *et al.*, "Multimodal validation of patient-specific intraventricular flow simulations from 4D echocardiography," in *Proc. IEEE Int. Ultrason. Symp.*, Tours, France, Sep. 2016, pp. 1–4.

[27] J. Hansegård, S. Urheim, K. Lunde, S. Malm, and S. I. Rabben, "Semi-automated quantification of left ventricular volumes and ejection fraction by real-time three-dimensional echocardiography," *Cardiovascular Ultrasound*, vol. 7, no. 1, p. 18, 2009.

[28] W. J. Schroeder, B. Lorensen, and K. Martin, "The visualization toolkit: Kitware," Kitware, Clifton Park, NY, USA, Tech. Rep. 1, 2004.

[29] A. Savitzky and M. J. E. Golay, "Smoothing and differentiation of data by simplified least squares procedures," *Anal. Chem.*, vol. 36, no. 8, pp. 1627–1639, 1964.

[30] J. Hoffman, J. Jansson, and M. Stöckli, "Unified continuum modeling of fluid-structure interaction," *Math. Models Methods Appl. Sci.*, vol. 21, no. 3, pp. 491–513, 2011.

[31] R. S. Rosenson, A. McCormick, and E. F. Uretz, "Distribution of blood viscosity values and biochemical correlates in healthy adults," *Clin. Chem.*, vol. 42, no. 8, pp. 1189–1195, 1996.

[32] E. S. D. Martino *et al.*, "Fluid-structure interaction within realistic three-dimensional models of the aneurysmatic aorta as a guidance to assess the risk of rupture of the aneurysm," *Med. Eng. Phys.*, vol. 23, no. 9, pp. 647–655, 2001.

[33] M. N. Frank and W. B. Kinlaw, "Indirect measurement of iso, volumetric contraction time and tension period in normal subjects," *Amer. J. Cardiol.*, vol. 10, no. 6, pp. 800–806, 1962.

[34] F. Arevalo and R. Sakamoto, "On the duration of the isovolumetric relaxation period (IVRP) in dog and man," *Amer. Heart J.*, vol. 67, no. 5, pp. 651–656, 1964.

[35] A. Logg and G. N. Wells, "DOLFIN: Automated finite element computing," *ACM Trans. Math. Softw.*, vol. 37, no. 2, p. 20, 2010.

[36] J. Hoffman *et al.*, "Unicorn: Parallel adaptive finite element simulation of turbulent flow and fluid–structure interaction for deforming domains and complex geometry," *Comput. Fluids*, vol. 80, pp. 310–319, Jul. 2013.

[37] M. D. Cerqueira *et al.*, "Standardized myocardial segmentation and nomenclature for tomographic imaging of the heart. A statement for healthcare professionals from the Cardiac Imaging Committee of the Council on Clinical Cardiology of the American Heart Association," *Circulation*, vol. 105, no. 4, pp. 539–542, 2002.

[38] E. Heiberg, J. Sjögren, M. Ugander, M. Carlsson, H. Engblom, and H. Arheden, "Design and validation of Segment-freely available software for cardiovascular image analysis," *BMC Med. Imag.*, vol. 10, no. 1, p. 1, 2010.

[39] T. Nordenfur *et al.*, "Algorithm comparison for cardiac image fusion of coronary computed tomography angiography and 3D echocardiography," in *Proc. IEEE Int. Ultrason. Symp.*, Taipei, Taiwan, Oct. 2015, pp. 1–4.

[40] R. Faludi *et al.*, "Left ventricular flow patterns in healthy subjects and patients with prosthetic mitral valves: An *in vivo* study using echocardiographic particle image velocimetry," *J. Thoracic Cardiovascular Surgery*, vol. 139, no. 6, pp. 1501–1510, 2010.

[41] J. O. Mangual *et al.*, "Comparative numerical study on left ventricular fluid dynamics after dilated cardiomyopathy," *J. Biomech.*, vol. 46, no. 10, pp. 1611–1617, 2013.

[42] G.-R. Hong *et al.*, "Characterization and quantification of vortex flow in the human left ventricle by contrast echocardiography using vector particle image velocimetry," *JACC, Cardiovascular Imag.*, vol. 1, no. 6, pp. 705–717, 2008.

[43] M. Courtois, S. Kovacs, and P. A. Ludbrook, "Transmitral pressure-flow velocity relation. Importance of regional pressure gradients in the left ventricle during diastole," *Circulation*, vol. 78, no. 3, pp. 661–671, 1988.

[44] R. Merrifield, Q. Long, X. Xu, P. J. Kilner, D. N. Firmin, and G.-Z. Yang, "Combined CFD/MRI analysis of left ventricular flow," in *Proc. Int. Workshop Med. Imag. Virtual Reality*, 2004, pp. 229–236.

[45] Q. Long, R. Merrifield, G. Z. Yang, X. Y. Xu, P. J. Kilner, and D. N. Firmin, "The influence of inflow boundary conditions on intra left ventricle flow predictions," *J. Biomech. Eng.*, vol. 125, no. 6, pp. 922–927, 2003.

[46] M. Nakamura, S. Wada, and T. Yamaguchi, "Influence of the opening mode of the mitral valve orifice on intraventricular hemodynamics," *Ann. Biomed. Eng.*, vol. 34, no. 6, pp. 927–935, 2006.

[47] T. M. Koelling, K. D. Aaronson, R. J. Cody, D. S. Bach, and W. F. Armstrong, "Prognostic significance of mitral regurgitation and tricuspid regurgitation in patients with left ventricular systolic dysfunction," *Amer. Heart J.*, vol. 144, no. 3, pp. 524–529, 2002.

[48] B. Baccani, F. Domenichini, and G. Pedrizzetti, "Model and influence of mitral valve opening during the left ventricular filling," *J. Biomech.*, vol. 36, no. 3, pp. 355–361, 2003.

[49] J. H. Seo *et al.*, "Effect of the mitral valve on diastolic flow patterns," *Phys. Fluids*, vol. 26, no. 12, p. 121901, 2014.

[50] E. Votta *et al.*, "Toward patient-specific simulations of cardiac valves: State-of-the-art and future directions," *J. Biomech.*, vol. 46, no. 2, pp. 217–228, 2013.

[51] V. Vedula, J.-H. Seo, A. C. Lardo, and R. Mittal, "Effect of trabeculae and papillary muscles on the hemodynamics of the left ventricle," *Theor. Comput. Fluid Dyn.*, vol. 30, nos. 1–2, pp. 3–21, 2014.

[52] S. N. Doost, L. Zhong, B. Su, and Y. S. Morsi, "The numerical analysis of non-Newtonian blood flow in human patient-specific left ventricle," *Comput. Meth. Programs Biomed.*, vol. 127, pp. 232–247, Apr. 2016.

[53] C. Jenkins, K. Bricknell, L. Hanekom, and T. H. Marwick, "Reproducibility and accuracy of echocardiographic measurements of left ventricular parameters using real-time three-dimensional echocardiography," *J. Amer. College Cardiol.*, vol. 44, no. 4, pp. 878–886, 2004.